

1. The angular absorption performance of the GST-Al and Cr-GST-Au structures are investigated and presented in Fig. S1. The absorption performance is robust to the incident angle in these two structures, even though the absorptivity and bandwidth change a little with the increase of the incident angle.

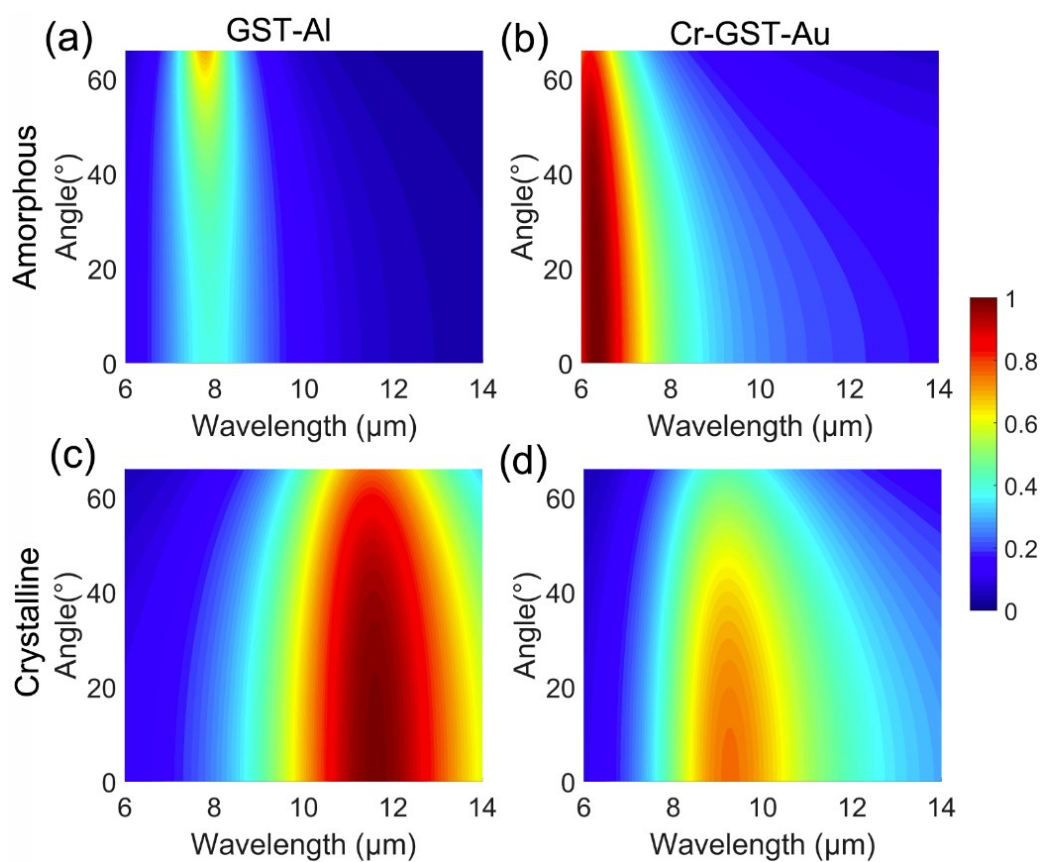


Fig. S1 The simulated absorptivity of the (a)aGST-Al (b)Cr-aGST-Au (c)cGST-Al(d)Cr-cGST-Au structure when incident angle increases from 0° to 60°.

2. The tunneling effect of the thin Cr layer in the Cr-GST-Au structure is dominating the high absorptivity during the tunable wavelength. The thickness of Cr layer have an effect on the peak wavelength and the peak emissivity. As shown in Fig. S2, a 2-nm-thick Cr layer is perfect for the wavelength-tunable thermal emitter with permanent high absorptivity/emissivity. However, the 2-nm-thick Cr layer is too thin to form a continuous film. In the experiment, a 5-nm-thick Cr layer is adopted.

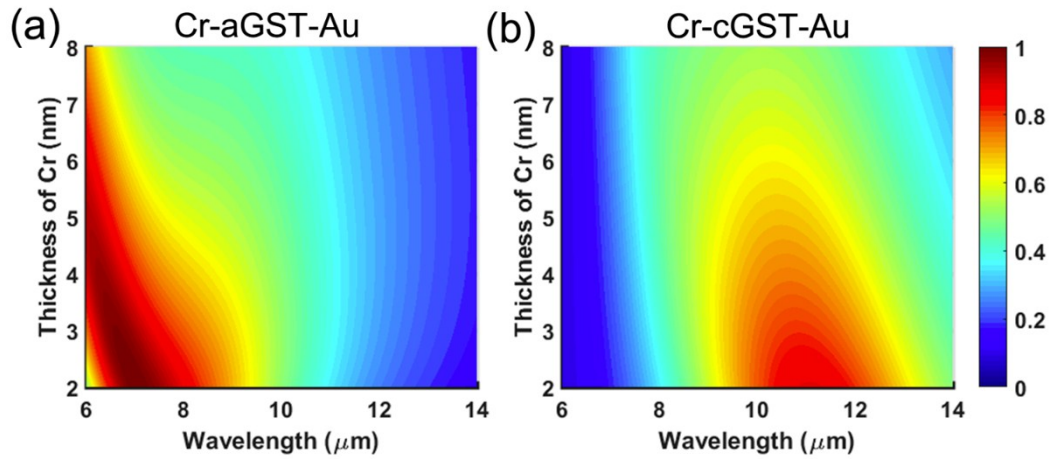


Fig. S2 The simulated absorptivity of the (a)Cr-aGST-Au and (b)Cr-cGST-Au structure when the thickness the Cr layer is changing from 2 nm to 8 nm.

3. The working band of the wavelength-tunable mid-infrared thermal emitter can be expanded to the other atmospheric window. To reach this goal, the thickness of the GST layer should be 200 nm and the bottom metal material should be changed. The GST-Pt and Au-GST-Au structures are adopted to realize high absorptivity during the wavelength change. The top Au layer is 3 nm.

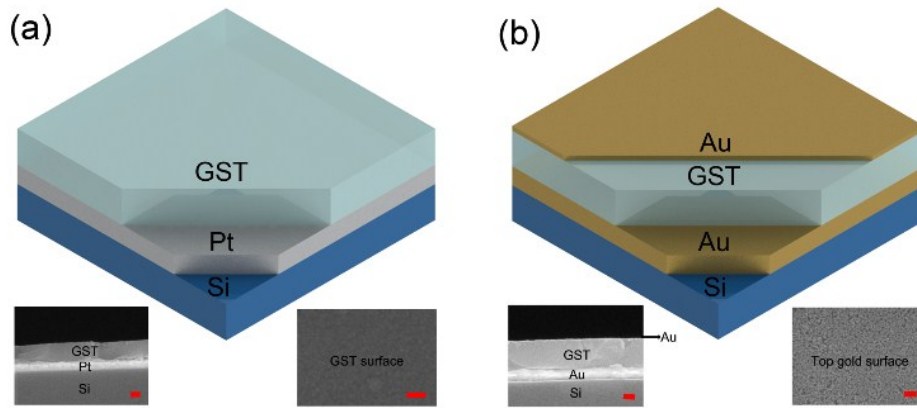


Fig. S3 Schematic diagrams and SEM images (both cross section and top view) of (a) the GST-Pt and (b) the Au-GST-Au MIR thermal sources. The scale bars in the SEM images are 100 nm.

4. The simulated absorptivity of the GST-Pt and Au-GST-Au structures as function of amorphous proportion and wavelength are studied (Fig. S4). For the GST-Pt structure, the peak absorption wavelength is $4.02\ \mu\text{m}$ at $X=1$ (amorphous phase) and increases to $5.76\ \mu\text{m}$ when X decreases to 0 (crystalline phase). The peak absorptivity remains above 0.6 during the whole phase transition process.

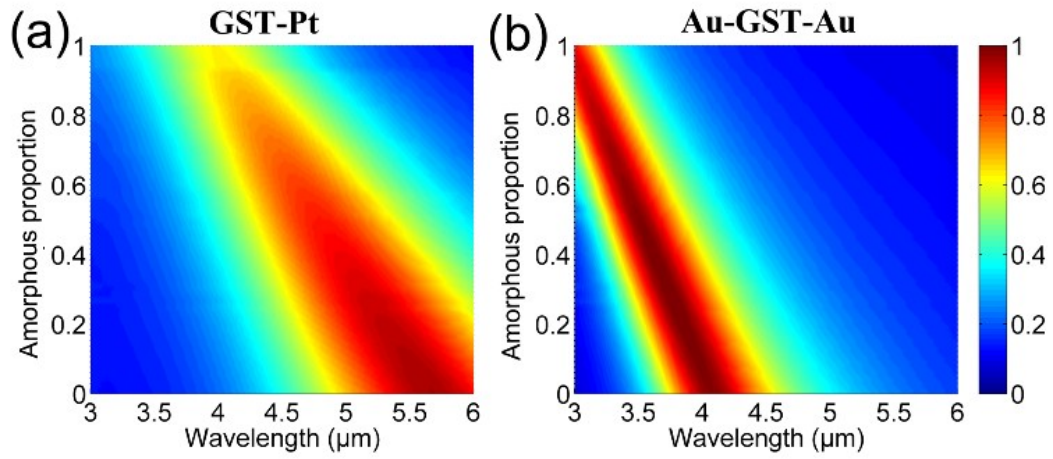


Fig. S4 The simulated absorptivity of the (a) GST-Pt and (b) Au-GST-Au MIR thermal sources for the wavelength range from $3\ \mu\text{m}$ to $6\ \mu\text{m}$ when varying the amorphous proportion from 0 to 1. The thickness of GST is 200 nm and the bottom metal is 100 nm in both structures. The surface Au layer is 3-nm-thick in the Au-GST-Au MIR thermal source.

5. The normalized electric field ($|E|$) and resistive loss (Q) distributions at the peak absorption wavelength for both amorphous and crystalline GST are investigated (Fig. S5).

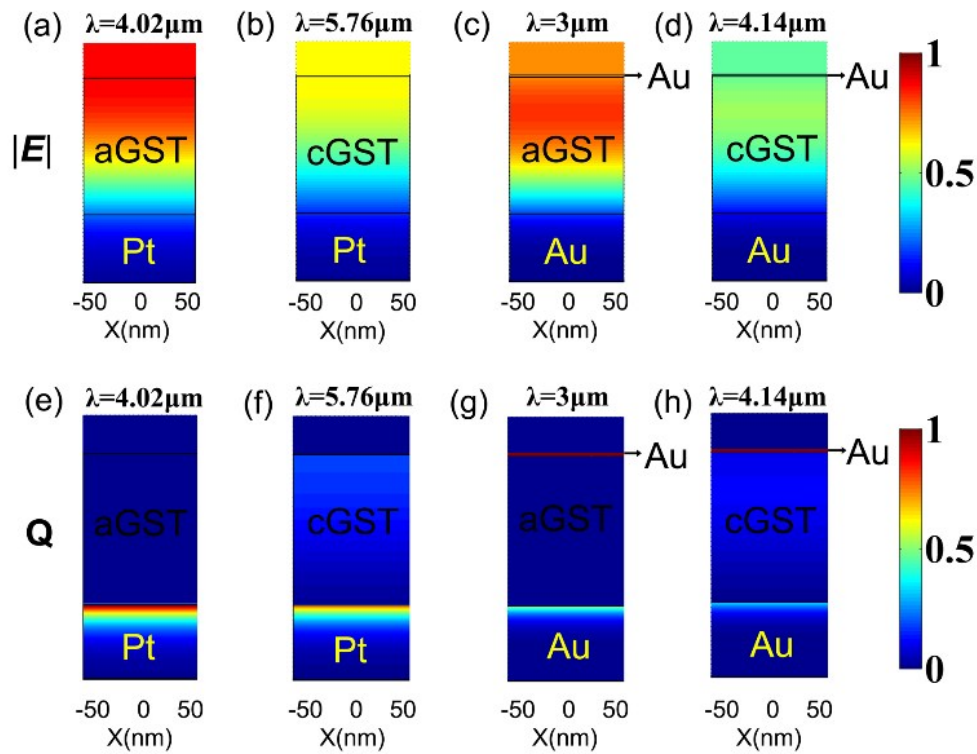


Fig. S5 The normalized electric field and resistive loss in the GST-Pt and Au-GST-Au MIR thermal sources at the peak absorption wavelength for amorphous and crystalline GST phases. The normalized electric field distributions (a-d) and resistive loss distributions (e-h) are presented for (a, e) aGST-Pt, (b, f) cGST-Pt, (c, g) Au-aGST-Au, and (d, h) Au-cGST-Au structures. The resistive loss in the top Au layer in (g) and (h) is not normalized as its intensity is far stronger than that in other parts.

6. The experimental performance of the devices is further investigated corresponding to the theoretical results discussed above. To compare with the GST-Al and Cr-GST-Au structure, similar thermal annealing methods are adopted in the GST-Pt and Au-GST-Au structure and the absorptivity of the structures are measured with FTIR.

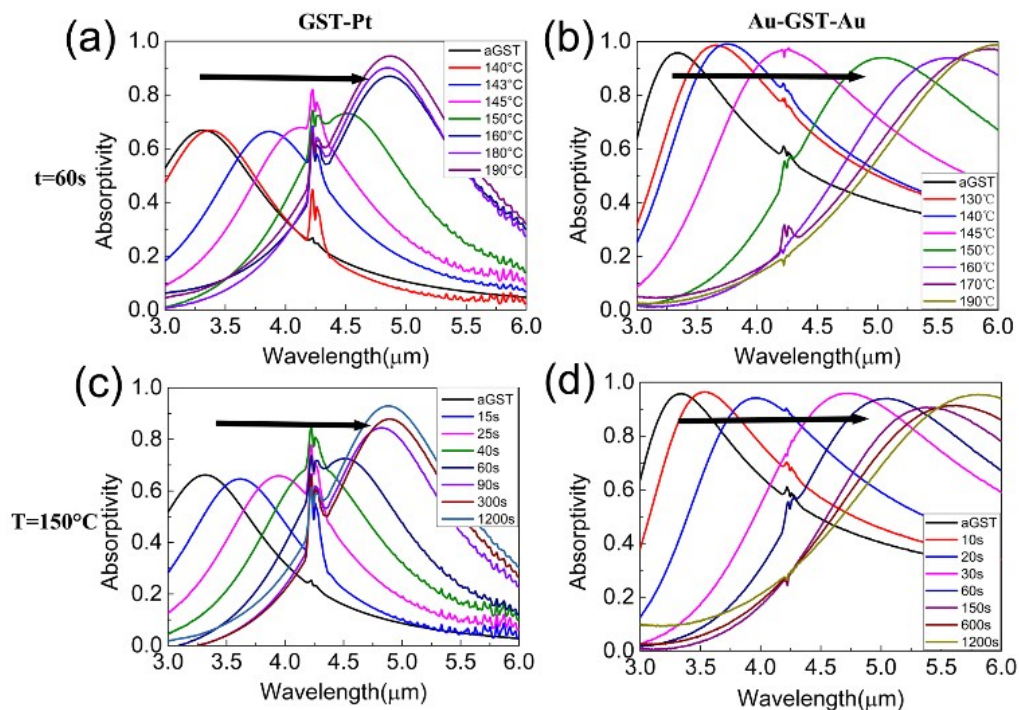


Fig. S6 The measured absorption spectra for the MIR thermal sources with two different annealing processes. (a) and (b) are for GST-Pt and Au-GST-Au structures annealed for 60 s at different annealing temperatures, respectively. (c) and (d) are for GST-Pt and Au-GST-Au structures annealed at 150 °C for different annealing time, respectively. The fluctuations at 4.25 μm are owing to the CO_2 absorption in the air.

7. The wavelength-tunable thermal emission performance of the GST-Pt and Au-GST-Au MIR thermal sources is further measured with FTIR. The peak emission wavelength for both the GST-Pt (Fig. S7a) and the Au-GST-Au (Fig. S7b) MIR thermal sources shifts to longer wavelength with higher annealing temperature or longer annealing time.

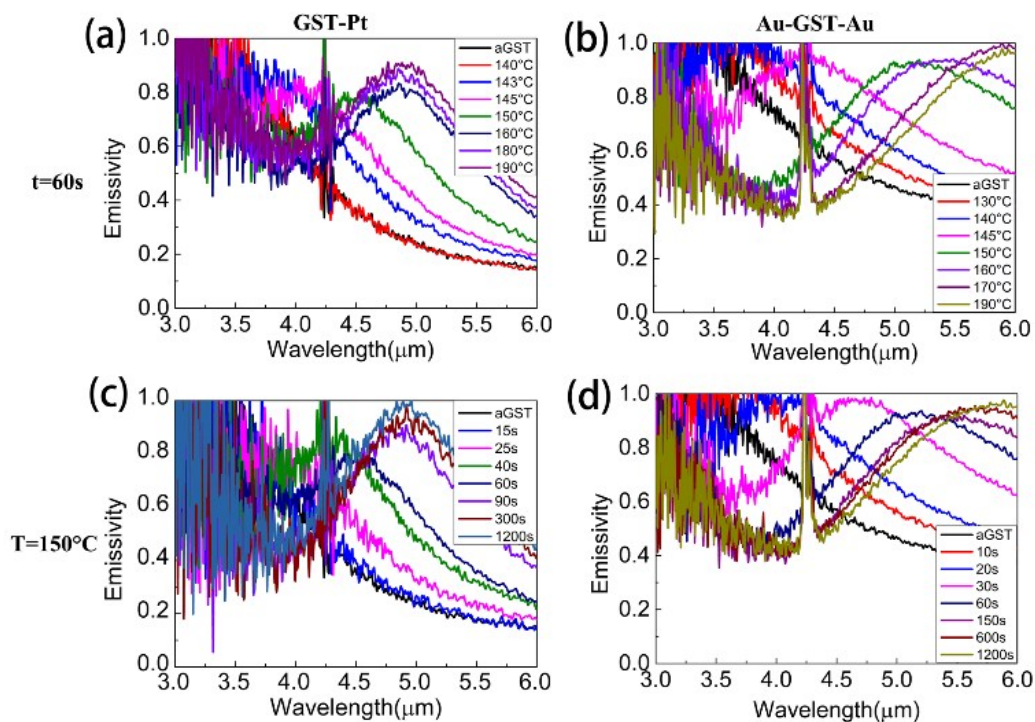


Fig. S7 The measured thermal emissivity curves at 100°C for the MIR thermal sources with different annealing time and temperatures. (a) and (b) are GST-Pt and Au-GST-Au MIR thermal sources annealed at different temperatures ($t=60\text{s}$), respectively. (c) and (d) are GST-Pt and Au-GST-Au MIR thermal sources annealed at different time ($T=150^\circ\text{C}$), respectively.